J Mater Sci: Mater Electron (2016) 27:1092–1099
DOI 10.1007/s10854-015-3856-8

Synthesis and optical properties of europium doped zinc silicate prepared using low cost solid state reaction method

Nur Alia Sheh Omar[1] · Yap Wing Fen[1,2] · Khamirul Amin Matori[1,2] · Mohd Hafiz Mohd Zaid[2] · Mohd Rasdi Norhafizah[1] · Mohammad Nurzilla[2] · Mohd Ismail Maisarah Zamratul[2]

Received: 13 May 2015 / Accepted: 6 October 2015 / Published online: 14 October 2015

Abstract This paper presents a study on synthesis and optical properties of Zn_2SiO_4:1 wt% Eu^{3+} at different heat treatments. The objective of the research is to synthesize Zn_2SiO_4:1 wt% Eu^{3+} phosphor by using low cost solid state reaction method with recycled waste bottle glasses as the silicate source. The X-ray diffraction results showed that the prepared Zn_2SiO_4:1 wt% Eu^{3+} phosphors have a sharp diffraction peak as the heat treatment temperatures were increased from 600 to 1000 °C. Furthermore, the morphology from the Field emission scanning electron microscope analysis were shown the formation of well crystalline samples with dense packed grains due to the increment of heat treatment temperatures. Fourier transform infrared spectra has confirmed the present elements in Zn_2SiO_4:1 wt% Eu^{3+} phosphors while the narrow width of Raman line spectra were observed at temperatures ranging from 700 to 1000 °C indicates good homogeneity and crystallinity of synthesized powders. In addition, the energy band gap of europium doped zinc silicate increased dramatically up to 3.62 eV at temperature of 1000 °C. Photoluminescence measurements has also exhibited the red emission corresponding to the $^5D_0 \rightarrow {}^7F_2$ (600 nm) when viewed under blue excitation.

1 Introduction

Among various host luminescent materials, zinc silicates (Zn_2SiO_4) have been identified as a very suitable host matrix to incorporate with rare earth ions and transition metal ions resulting in an excellent luminescence in the blue, green and red spectral zones [1–5]. With modern technology, rare earth ions are better candidates for luminescence activators in phosphor materials than transition metals [6]. They have completely filled $4f$ shells, well shielded by $5s^2$ and $5p^6$ orbitals and their emission transitions yield sharp lines in the optical spectra providing phosphors with high luminescence efficiency [7, 8]. Besides that, rare earth (RE) ions also have an attractive role as active ions in many optical materials due to a large number of the absorption and emission bands arising from the transitions between the energy levels. Owing to these factors, many researchers focused their attention on trivalent europium ions as a luminescence centres in intense red emission coming from its $^5D_0$–$^7F_2$ transition [9–13]. Presently, europium (Eu^{3+}) ion is one of the most popular and important rare-earth dopants because Eu^{3+}-doped

✉ Yap Wing Fen
yapwingfen@upm.edu.my

Nur Alia Sheh Omar
nuralia.upm@gmail.com

Khamirul Amin Matori
khamirul@upm.edu.my

Mohd Hafiz Mohd Zaid
mhmzaid@gmail.com

Mohd Rasdi Norhafizah
hafiezah91@gmail.com

Mohammad Nurzilla
nurzilla@gmail.com

Mohd Ismail Maisarah Zamratul
zamrah48@gmail.com

[1] Institute of Advanced Technology, Universiti Putra Malaysia, 43400 UPM Serdang, Selangor, Malaysia

[2] Department of Physics, Faculty of Science, Universiti Putra Malaysia, 43400 UPM Serdang, Selangor, Malaysia

phosphors are well known to be promising materials for electroluminescent devices, optical amplifiers, and lasers [14, 15]. Several methods have been developed to prepare Zn_2SiO_4:Eu^{3+} such as conventional solid state reaction, sol gel synthesis, co-precipitation synthesis, spray pyrolysis and hydrothermal method [16, 17]. As a comparison, the conventional solid states methods have targeting a better simplicity in the industrial operation than chemical method [18, 19]. However, this method is usually used highly cost of SiO_2 source to synthesizing the zinc silicate. In order to overcome the drawback, it is needed to develop a new silicate sources from waste soda lime silica (SLS) glasses for cost saving. The soda lime silicate glass has been found to be a suitable optical material with high transparency, low melting point, high thermal stability and good rare-earth ion solubility [20, 21].

Thus, this paper would show the study about the synthesis and optical properties of Eu^{3+} doped Zn_2SiO_4 phosphor by using low cost solid state reaction method. Effects of 1 wt% Eu_2O_3 by varying the heat treatment temperature of Eu^{3+} ions in Zn_2SiO_4 on the optical properties were investigated.

2 Materials and methods

2.1 Synthesis

The synthesis process of 1 wt% europium doped Zn_2SiO_4 based glass ceramics was prepared using conventional melt quenching in water technique. The starting materials are zinc oxide [ZnO (99.00 %)], soda lime silica (SLS) glass form waste bottle glasses and europium oxide [Eu_2O_3 (99.99 %)] were used in this experiment. The chemical batch of ZnO, waste SLS glass, 1 wt% europium was mixed together via milling process for 24 h using a ball milling jar, and then was melted at 1400 °C for 2 h. The molten mixture was poured into the water to get the glass fritz. Then the glass fritz was cooled to room temperature and then was crushed and sieved into fine powder about 63 microns. After the addition of 1.75 wt% polyvinyl alcohol (PVA) binders, the powders have been pressed at a pressure of 5 tons for 15 min to form the pellets and were sintered at different temperatures from 600 to 1000 °C.

2.2 X-ray diffraction (XRD)

The amorphous and crystalline phase of the samples were investigated from X-ray diffraction spectrum recorded on a Phillips X'pert X-ray Diffractometer and the data were collected over the 2θ range 10°–80° at room temperature. The data then analysed by utilizing software X'pert HighScore.

2.3 Field emission scanning electron microscopy (FESEM)

The field emission scanning electron microscopy was carried out on the samples coated with gold (Au) to observe the surface morphology of the obtained glasses and glass ceramics using Nova NanoSEM 30 Series under high vacuum.

2.4 Fourier transforms infrared spectroscopy (FTIR)

The infrared (IR) absorption measurements on the samples were made by employing the KBr pellet technique. The IR spectra were recorded at room temperature in the range 550–4000 cm^{-1} using VERTEX 70 instrument for identifying the chemical bonding of the samples.

2.5 Raman spectroscopy

Raman spectra were recorded on Witec Raman spectroscopy, model Alpha 300R using He–Ne laser with 532.390 nm as excitation source.

2.6 Ultraviolet–visible (UV–Vis) spectroscopy

The UV–visible absorption spectra measurements in the wavelength range 250–800 nm were performed at room temperature by using Shimadzu UV–Vis–NIR spectroscopy. In addition, the absorption edge for all samples was also observed to calculate the optical band gaps energy of the materials.

2.7 Photoluminescence (PL)

Photoluminescence excitation and emission spectra were performed at room temperature by using Perkin Elmer LS 55 Fluorescence spectrometer. The emission spectra are obtained by excitation at 400 nm and the excitation spectra are obtained by emission at 600 nm.

3 Results and discussion

3.1 X-ray diffraction (XRD)

The X-ray diffraction pattern of the 1 wt% Eu^{3+} doped Zn_2SiO_4 precursor glass and Zn_2SiO_4 glass ceramics are shown in Fig. 1. There is no diffraction peak appeared in

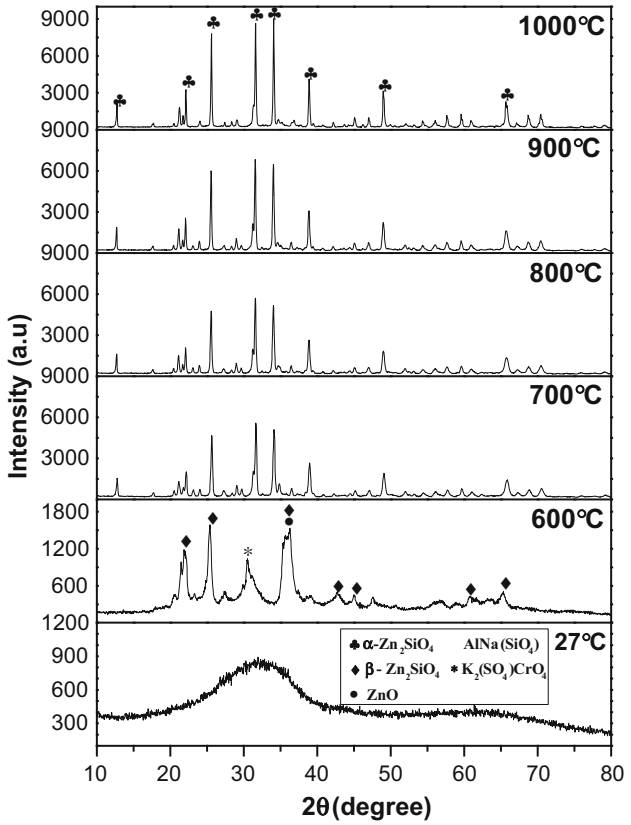

Fig. 1 X-ray diffraction pattern of Zn_2SiO_4:1 wt% Eu^{3+}

the precursor glass which indicates that this sample is amorphous in nature. Then, the XRD patterns revealed well-developed of major β-Zn_2SiO_4 (JCDPS file 14-0653) phase diffraction peaks with a minor peak of ZnO (JCPDS card No. 36-1451) as the prepared samples were heat treated at 600 °C. Also some additional peaks corresponding to those of $AlNa(SiO_4)$ (JCPDS card No. 02-0625) and $K_2(SO_4)CrO_4$ (JCPDS card No. 25-1236) could be noticed at this temperature. As the temperature further increased to 1000 °C, the β-Zn_2SiO_4 phase was completely transformed to α-Zn_2SiO_4, which corresponds to JCDPS file 37-1485 and the minor phases of ZnO, $AlNa(SiO_4)$ and $K_2(SiO_4)CrO_4$ disappeared [22, 23]. It is found that the intensity of diffraction peaks get higher and sharper with the increase of heat treatment temperatures. In XRD pattern, broader peaks were caused due to smaller crystallite sizes and sharp peaks due to the formation of comparatively larger crystallites. The increased of heat treatment temperatures have attributed to the improved crystallinity [24–26]. From the heat treatment temperature of 800 °C, the samples displayed a good crystallization. At higher treatment of sintering, diffusion ions in the glasses are increased, hence the crystal growth rate is accelerated and larger crystals result in the glass matrix [27, 28].

3.2 Field emission scanning electron microscopy (FESEM)

The surface morphology of the Zn_2SiO_4:1 wt% Eu^{3+} is shown in Fig. 2. From the micrographs, it is clearly observed that the surface morphology of the particles was not uniform and the grains are irregular in shape. The particles tend to aggregate, strongly showing good connectivity between grains. Moreover, the agglomeration of powder particles was also observed. From the FESEM image, it can be observed that the morphology of particles changes depending on the temperature [29–31]. As the sintering temperature increase, sample decrease of the porosity showing that the ceramic consists of closely packed grains and lead to produce a bit larger ceramics [32–34]. Furthermore, at higher temperature of sintering, the particles are no longer in irregular in shapes as well as the particle are tends to be seen in circular in shapes and coalescent together which have been shown in Fig. 2d, e, indicating that well crystallized ceramics.

3.3 Fourier transforms infrared (FTIR) spectroscopy

The quality and composition of different sintering temperature for Zn_2SiO_4:1 wt% Eu^{3+} was characterized by FTIR spectroscopy at room temperature in the range 500–4000 cm^{-1} (Fig. 3). All FTIR spectra of samples are very similar regardless the heat treatment of temperature of the material. The FTIR spectrum of Zn_2SiO_4:1 wt% Eu^{3+} contains clearly exhibits broad bands in the region ($\sim$3443.57 cm^{-1}) of hydroxyl group show the stretching vibration of O–H groups [34]. Note that these broad peaks become weaker with increasing heat treatment temperature. Hence, the sintering process has proven to be suitable to remove all the organic molecules and OH groups which enable the samples to be more promising luminescent materials. The strong band was observed in the 980 cm^{-1} and below was due to SiO_4 asymmetric stretching vibration. The peak in the $\sim$650 cm^{-1} was ascribed to the bonding of Zn–O–Si symmetric stretching [26]. The peak in the lower wavenumber at $\sim$530 cm^{-1} was attributed to the ZnO symmetric stretching in ZnO_4 group [35, 36]. The absorption peaks of SiO_4 (asymmetric) and ZnO_4 become stronger due to increasing heat treatment temperature, suggesting crystallization of Zn_2SiO_4 crystal in the glass matrix was formed [37].

3.4 Raman spectroscopy

Figure 4 presents Zn_2SiO_4 powder phosphor doped 1 wt% Eu^{3+} that has been sintered from 600 to 1000 °C by a solid state reaction method. As seen from the figure, the

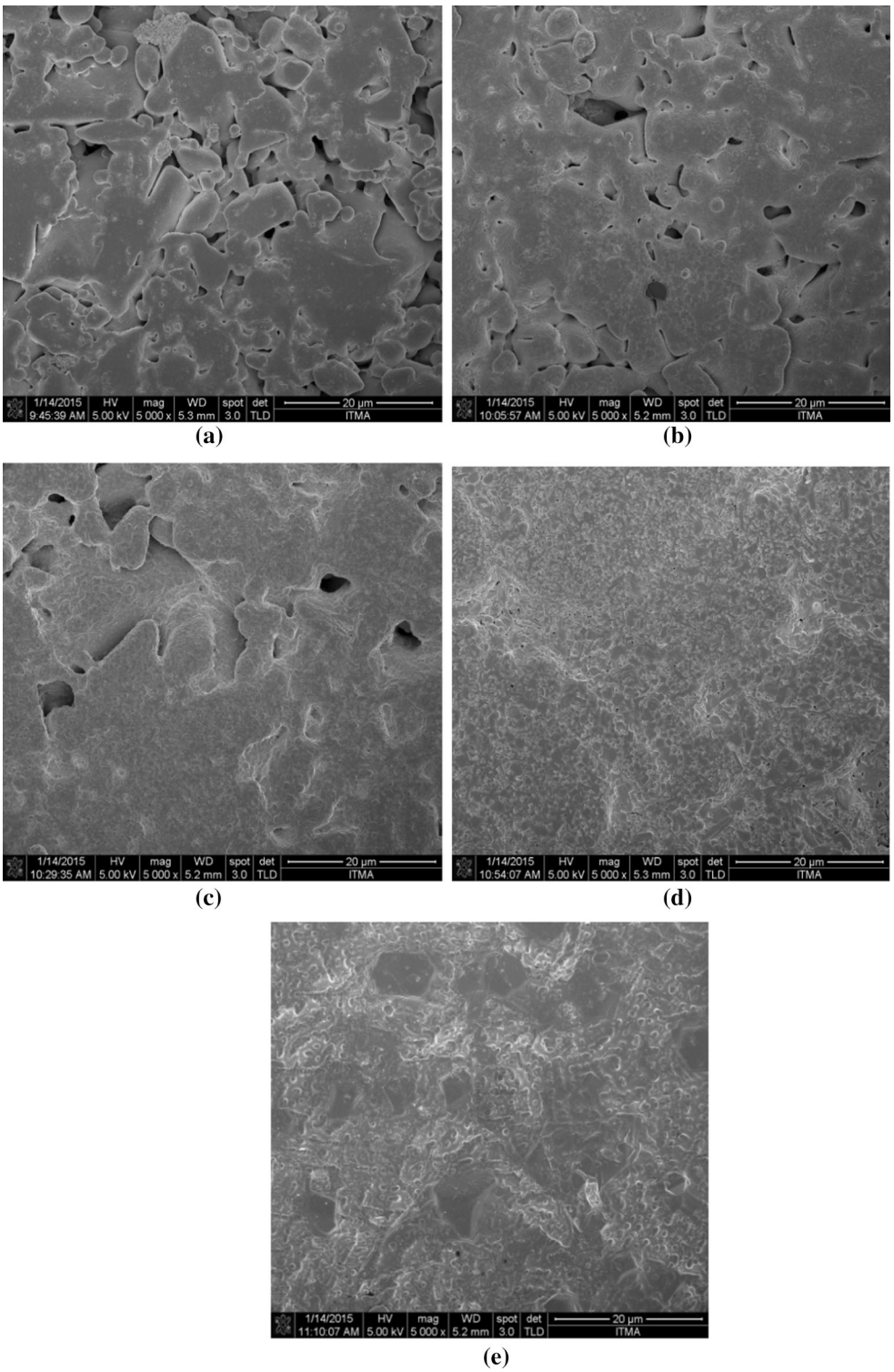

Fig. 2 FESEM images of Zn_2SiO_4:1 wt% Eu^{3+} samples heat treatment at **a** 600 °C, **b** 700 °C, **c** 800 °C, **d** 900 °C, **e** 1000 °C

spectrum of this sample powder possesses the strong Raman peaks at 2500–3000 cm^{-1} is attributed to strong C–H vibrational features. Besides, a broad scattering peak at 1700–1900 cm^{-1} exhibited of hydroxyl group show the stretching vibration of O–H groups. The weak Raman band in the 900–1500 cm^{-1} region has been assigned to the stretching vibrations of the SiO_4 group [26]. The sharpness and intensity of the bands can be an indication of the

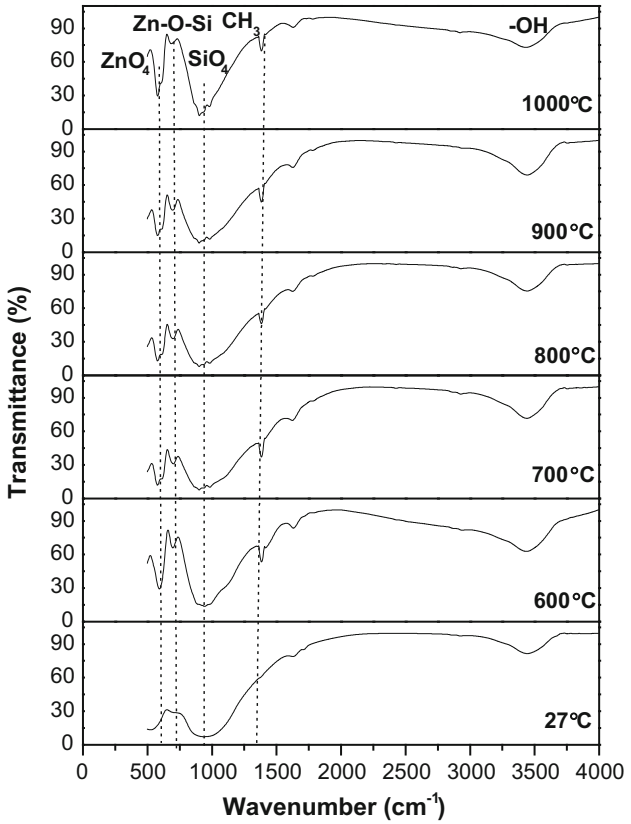

Fig. 3 FTIR spectra of Zn_2SiO_4:1 wt% Eu^{3+}. *Lines* are drawn to guide the eye

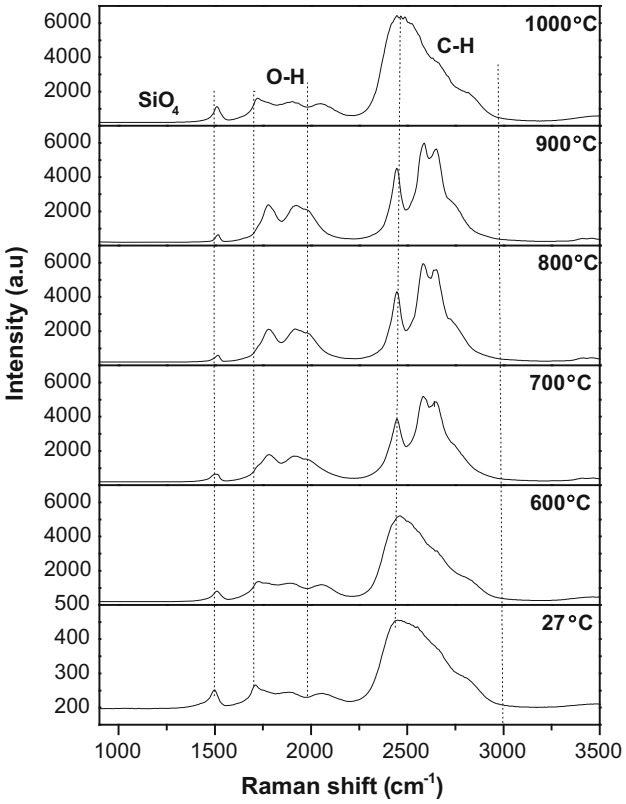

Fig. 4 Raman spectra of Zn_2SiO_4:1 wt% Eu^{3+}. *Lines* are drawn to guide the eye

crystallinity of the sample powders. The Raman band of un-sintered sample has showed the lowest intensity which indicates that the sample is mainly amorphous. The intensity of the broad band start to increase as the heat treatment temperature occurs at 600 °C. It was found that the sample powder at 600 °C is less crystalline than other heat treatment temperature [32]. The narrow width of Raman lines spectra of heat treatment temperature of 700–1000 °C indicates good homogeneity and crystallinity of synthesized powders which shows a good agreement with X-ray diffraction, FTIR, and FESEM result [38].

3.5 Optical absorption measurements

3.5.1 Absorbance versus wavelength

UV–Vis spectroscopy was used to characterize the optical absorbance of the Zn_2SiO_4:1 wt% Eu^{3+}. Figure 5 shows the absorption spectrum of Eu^{3+} doped Zn_2SiO_4 in the spectral region from 200 to 800 nm at room temperature. The absorption profiles exhibit broad bands in the UV region (below 400 nm). Additionally, the absorbance spectra of all heat treatment temperatures are very similar. It was found that the absorption spectra of heat-treated

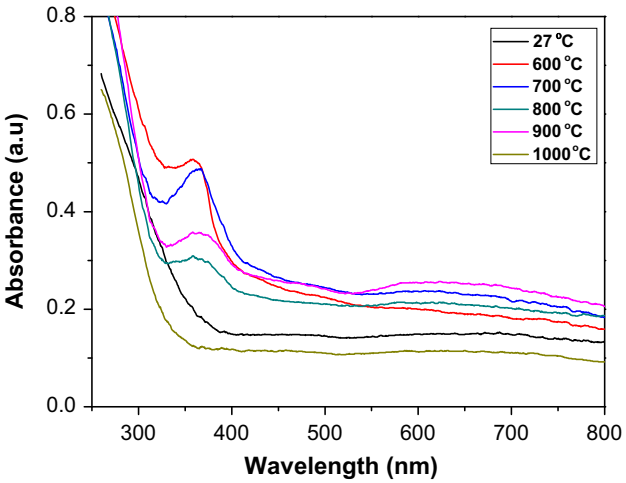

Fig. 5 Absorption spectra of Zn_2SiO_4:1 wt% Eu^{3+}

samples are uplifted due to scattering by the Zn_2SiO_4 crystals [39].

3.5.2 Optical band gap

The absorption spectra of Eu^{3+} doped Zn_2SiO_4 were carried out to resolve the valence–conduction band transition,

which allows us to calculate the band gap. UV–Vis spectra indicate Zn_2SiO_4 single crystal is estimated has an optical band gap of 5.5 eV [40]. The Fig. 6 depicts that the Zn_2SiO_4:1 wt% Eu^{3+} has optical band gap energy (E_{gap}) of 3.20 eV before induces a heat treatment. The relation between the absorption coefficient (α) and incident photon energy (hν) for the case of indirect transition of Zn_2SiO_4 has a characteristic relation [41]:

$$(\alpha h\nu)^{1/2} = k\left[h\nu - E_{gap}\right] \quad (1)$$

where k is constant, and E_{gap} is the optical energy gap of the material. By extrapolating the linear portion of the optical absorption curve or its tail, it is possible to verify that indirect energy band gap value for 600, 700, 800, 900 and 1000 °C is 2.94, 2.73, 2.62, 2.54 and 3.62 eV, respectively.

Figure 7 displays the variation of the energy band gap, E_{gap} with heat treatment temperatures of Zn_2SiO_4:1 wt% Eu^{3+}. The values of the energy band gap decreased linearly as the heat treatment temperature of Zn_2SiO_4:1 wt% Eu^{3+} increases from 600 to 900 °C which were range from 2.94 to 2.54 eV. This variation can be noted that the heat treatment at higher temperature induces a red shift of the electronic absorption edge towards larger wavelength indicating to smaller energy band gap produced which related to glass crystallization process [42]. However, the energy band gap is dramatically increased to 3.62 eV at 1000 °C. This might be due to the stabilized orthorhombic phase and improved crystallinity of the sample, thus, increased band gap by widening the absorption edge [43].

3.5.3 Photoluminescence

The results of photoluminescence excitation spectroscopy for Zn_2SiO_4:1 wt% Eu^{3+} glass and glass ceramics are shown in Fig. 8. The excitation spectra show five distinguished characteristics peaks centred at ~400, 414, 460, 500, and 527 nm which are transitions from the ground state ($^7F_0$) to the indicated excited levels [44]. The most prominent peak, located at 400 nm which are assigned to the transitions $^7F_0 \rightarrow {}^5L_6$. In the following, this peak was used to record Eu^{3+} emission spectra (Fig. 9).

The emission spectra under blue light (400 nm) excitation reveal five characteristics emission bands at ~527, 575, 600, 653, and 725 nm which are assigned to $^5D_1 \rightarrow {}^7F_1$, $^5D_0 \rightarrow {}^7F_1$, $^5D_0 \rightarrow {}^7F_2$, $^5D_0 \rightarrow {}^7F_3$, and $^5D_0 \rightarrow {}^7F_4$ electronic transitions of Eu^{3+} ion, respectively. The red emission peak is found at 600 nm ($^5D_0 \rightarrow {}^7F_2$) is attributed to the hypersensitive forced electric dipole transitions of Eu^{3+} and it is found dominant over emission

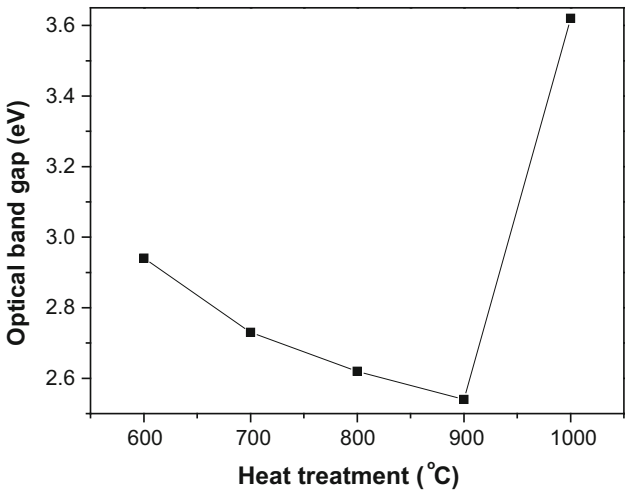

Fig. 7 Relationship between optical band gap heat treatments of Zn_2SiO_4:1 wt% Eu^{3+}

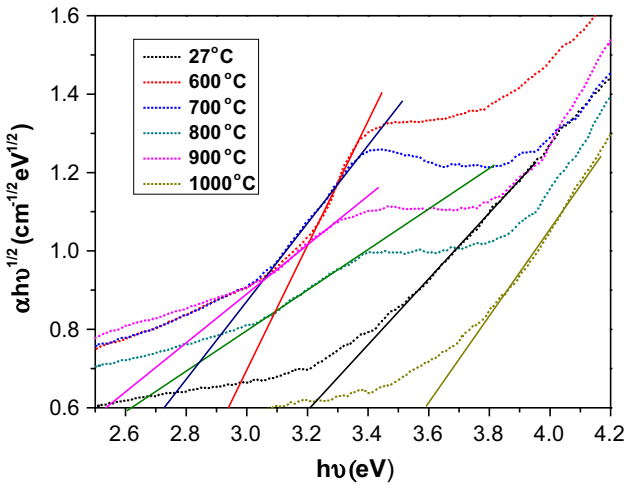

Fig. 6 Plot of $(\alpha h\nu)^{1/2}$ against hν for sample Zn_2SiO_4:1 wt% Eu^{3+}

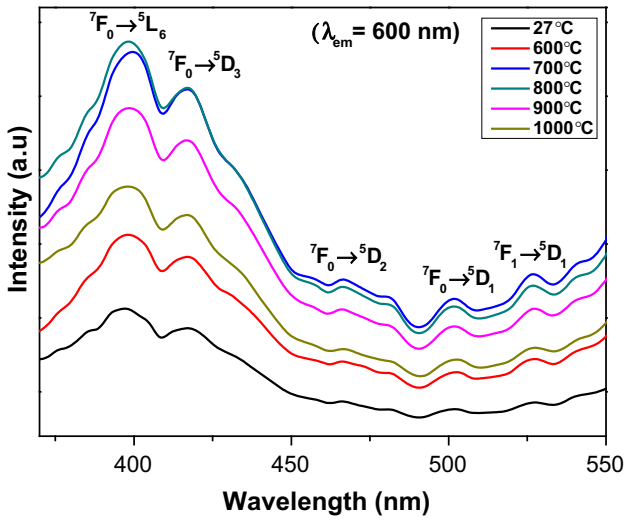

Fig. 8 Excitation spectra of Zn_2SiO_4:1 wt% Eu^{3+} (λ_{em} = 600 nm)

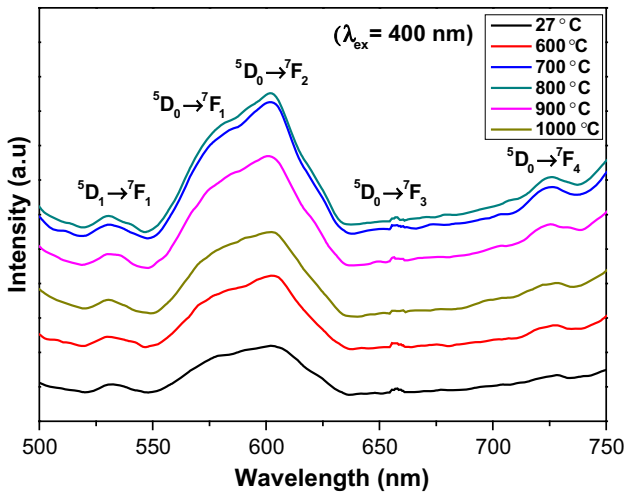

Fig. 9 Emission spectra of Zn_2SiO_4:1 wt% Eu^{3+} (λ_{em} = 400 nm)

peak at 575 nm ($^5D_0 \rightarrow {}^7F_1$) which is attributed to magnetic dipole transitions [35, 45, 46]. As seen in Fig. 9, the emission intensity of $^5D_0 \rightarrow {}^7F_j$ transition is uplifted after sintering temperature up to 600 °C and then decreased when the sintering temperature getting high due to improvement of crystallinity [47].

4 Conclusion

A solid state reaction method was employed to prepare Eu^{3+} doped Zn_2SiO_4 with different heat treatments, and their structure, morphology and optical properties were discussed as well. The sintered prepared samples show the materials have high crystalline and having sharp peaks compared to un-sintered. Results indicate that the progress of heat treatment leads to an increase in diffraction peak intensity. The FESEM analysis revealed that the 1 wt% Eu doped zinc silicate having well crystalline and aggregated tightly with each other due to the high temperature of heat treatment at 900 and 1000 °C. Besides, the narrow width of Raman lines spectra of heat treatment temperature of 700–1000 °C indicates good homogeneity and crystallinity of synthesized powders which shows a good agreement with XRD, FTIR, and FESEM results. The sintered samples exhibit decreasing energy band gap as heat treatment temperatures increased up to 900 °C and then, increased dramatically to 3.62 eV when the heat treatment temperatures extended to 1000 °C. The results of photoluminescence gives a red luminescence emission at 600 nm due to Eu^{3+} intraionic transitions under 400 nm excitation.

Acknowledgments The authors gratefully acknowledge the financial support for this study from the Malaysian Ministry of Education (MOE), Ministry of Science, Technology and Innovation (MOSTI) and Universiti Putra Malaysia through Fundamental Research Grant Scheme (FRGS), Science Fund, and Putra Grant. The laboratory facilities provided by the Functional Devices Laboratory, Institute of Advanced Technology, Universiti Putra Malaysia, are also acknowledged.

References

1. A. Patra, G.A. Baker, S.N. Baker, Opt. Mater. **27**, 15 (2004)
2. A.G. Joly, W. Chen, J. Zhang, S. Wang, J. Lumin. **126**, 491 (2007)
3. L.J. Dacanin, S.R. Lukic, D.M. Petrovic, M. Nikolic, M.D. Dramicanin, Phys. B **406**, 2319 (2011)
4. H. Huang, B. Yan, Appl. Surf. Sci. **252**, 2967 (2006)
5. H.X. Zhang, C.H. Kam, Y. Zhou, X.Q. Han, S. Buddhudu, Y.L. Lam, C.Y. Chan, Thin Solid Films **370**, 50 (2000)
6. R. Krsmanovic, Z. Antic, M.M. Cincovic, M.D. Dramicanin, J. Optoelectron. Adv. Mater. Symp. **1**, 37 (2009)
7. H.X. Zhang, S. Buddhudu, C.H. Kam, Y. Zhou, Y.L. Lam, K.S. Wong, B.S. Ooi, S.L. Ng, W.X. Que, J. Mater. Chem. Phys. **68**, 31 (2001)
8. B.V. Padlyak, I.I. Kindrat, V.O. Protsiuk, A. Drzewiecki, Ukr. J. Phys. Opt. **15**, 103 (2014)
9. M.M. Cincovic, B. Jankovic, B. Milicevic, Z. Antic, R.K. Whiffen, M.D. Dramicanin, Powder Technol. **249**, 497 (2013)
10. G. Gao, S. Reibstein, M. Peng, L. Wondraczek, J. Mater. Chem. **21**, 3156 (2011)
11. H. Li, B.K. Moon, B.C. Choi, J.H. Jeong, H.K. Yang, J. Kiwan, H.S. Lee, S.S. Yi, J. Mater. Chem. Phys. **139**, 998 (2013)
12. M.A.K. Elfayoumi, M. Farouk, M.G. Brik, M.M. Elokr, J. Alloys Compd. **492**, 712 (2010)
13. S.S. Rojas, J.E.D. Souza, K. Yukimitu, A.C. Hernandes, J. Non-Cryst. Solids **398**, 57 (2014)
14. D.T.M. Huong, N.H. Nam, L.V. Vu, N.N. Long, J. Alloys Compd. **537**, 54 (2012)
15. J. Yang, X. Li, J. Lang, M. Wei, M. Gao, X. Liu, H. Zhai, R. Wang, Y. Liu, J. Cao, Mater. Sci. Semicond. Process. **14**, 247 (2011)
16. R.Y. Yang, Y.M. Peng, H.L. Lai, C.J. Chu, B. Chiou, Y.K. Su, Opt. Mater. **35**, 1719 (2013)
17. L.K. Bharat, Y.I. Jeon, J.S. Yu, J. Alloys Compd. **614**, 443 (2014)
18. C. Li, Z. Liang, H. Xiao, Y. Wu, Y. Liu, J. Mater. Lett. **64**, 1972 (2010)
19. R.K. Tamrakar, D.P. Bisen, N. Brahme, J. Radiat. Res. Appl. Sci. **7**, 550 (2014)
20. P. Chimalawong, K. Kirrdsiri, J. Kaewkhao, P. Limsuwan, Proc. Eng. **32**, 690 (2012)
21. P. Chimalawong, J. Kaewkho, C. Kedkaew, P. Limsuwan, J. Phys. Chem. Solids **71**, 965 (2010)
22. B. Yang, H. Huang, J. Alloys Compd. **429**, 338 (2007)
23. V. Natarajan, K.V.R. Murthy, M.L.J. Kumar, Solid State Commun. **134**, 261 (2005)
24. R. Gunawidjaja, T. Myint, H. Eilers, J. Solid State Chem. **184**, 3280 (2011)
25. S. Kamei, Y. Kojima, N. Nishimiya, J. Lumin. **130**, 2247 (2010)
26. B.C. Babu, S. Buddhudu, J. Spectrosc. Dyn. **4**, 1 (2014)
27. A. Tarafder, A.R. Molla, S. Mukhopadhyay, B. Karmakar, Opt. Mater. **36**, 1463 (2014)
28. V.B. Taxak, Sheetal, Dayawati, S.P. Khatkar, Curr. Appl. Phys. **13**, 594 (2013)
29. I.P. Sahu, D.P. Bisen, N. Brahme, R.K. Tamrakar, J. Radiat. Res. Appl. Sci. **8**, 104 (2014)
30. G. Braziulis, R. Stankeviciute, A. Zalga, Mater. Sci. **20**, 90 (2014)

31. M. Ayvacikli, A. Ege, S. Yerci, N. Can, J. Lumin. **131**, 2432 (2011)
32. N.V. Pillai, V.P.M. Pillai, R. Vinodkumar, I. Navas, V. Ganesan, P. Koshy, J. Alloys Compd. **509**, 2745 (2011)
33. L. Qin, C. Xu, Y. Huang, S.I. Kim, H.J. Seo, Ceram. Int. **40**, 1605 (2014)
34. C.N. Raju, S. Sailaja, S.H. Raju, S.J. Dhoble, U. Rambabu, Y.D. Jho, B.S. Reddy, Ceram. Int. **40**, 7701 (2014)
35. P.V. Ramakrishna, D.B.R.K. Murthy, D.L. Sastry, Spectrochem. Acta Part A Mol. Biomol. Spectrosc. **125**, 234 (2014)
36. S.A. Al Rifai, B.A. Kulnitsky, J. Phys. Chem. Solids **74**, 1733 (2013)
37. P.V. Ramakrishna, D.B.R.K. Murthy, D.L. Sastry, K. Samatha, Spectrochem. Acta Part A Mol. Biomol. Spectrosc. **129**, 274 (2014)
38. I.E. Kolesnikov, D.V. Tolstikova, A.V. Kurochkin, A.A. Manshina, M.D. Mikhailov, Opt. Mater. **37**, 306 (2014)
39. A. Tarafder, A.R. Molla, C. Dey, B. Karmakar, J. Am. Ceram. Soc. **96**, 2424 (2013)
40. Q.Y. Zhang, K. Pita, C.H. Kam, J. Phys. Chem. Solids **64**, 333 (2003)
41. G. Wang, Y. Yang, Q. Mu, Y. Wang, J. Alloys Compd. **498**, 81 (2010)
42. S.A. Lourenco, N.O. Dantas, E.O. Serqueira, W.E.F. Ayta, A.A. Andrade, M.C. Filadelpho, J.A. Sampaio, M.J.V. Bell, M.A. PereiradaSilva, J. Lumin. **131**, 850 (2011)
43. G.S.R. Raju, E. Pavitra, G. Nagaraju, J.S. Yu, Dalton Trans. **44**, 1790 (2015)
44. B.P. Singh, A.K. Parchur, R.S. Ningthoujam, A.A. Ansari, P. Singh, S.B. Rai, Dalton Trans. **43**, 4779 (2013)
45. R.J. Wiglusz, T. Grzyb, A. Watras, P.J. Deren, S. Lis, W. Strek, J. Rare Earths **29**, 1105 (2011)
46. B.P. Singh, Maheshwary, P.V. Ramakrishna, S. Singh, V.K. Sonu, S. Singh, P. Singh, A. Bahadur, R.A. Singh, S.B. Rai, RSC Adv. **5**, 55977 (2015)
47. J. Li, M. Kuwabara, Sci. Technol. Adv. Mater. **4**, 143 (2003)